Crystallite size-dependent phases in nanocrystalline ZrO_2–Sc_2O_3

Paula M. Abdala,[a] Márcia C. A. Fantini,[b] Aldo F. Craievich[b] and Diego G. Lamas*[a]

Received 28th October 2009, Accepted 22nd December 2009
First published as an Advance Article on the web 27th January 2010
DOI: 10.1039/b922541b

ZrO_2-10, 12 and 14 mol% Sc_2O_3 nanopowders were prepared by using a nitrate-lysine gel-combustion synthesis. These materials were studied by synchrotron X-ray powder diffraction (SXPD) and Raman spectroscopy after calcination at different temperatures from 650 to 1200 °C, which led to samples with different average crystallite sizes, up to about 100 nm. The results from SXPD and Raman analyses indicate that, depending on Sc_2O_3 content, the metastable t′′-form of the tetragonal phase or the cubic phase are fully retained at room temperature in nanocrystalline powders, provided an average crystallite sizes lower than ~30 nm. By contrast, powders with larger average crystallite sizes exhibit the stable rhombohedral, β and γ, phases and do not retain or very partially retain the metastable t′′ and cubic ones.

Introduction

Zirconia-based ceramics are intensely investigated because of their excellent electrical and mechanical properties. They are used in many electrochemical devices such as solid-oxide fuel cells, oxygen sensors, oxygen pumps, *etc*. In particular, ZrO_2–Sc_2O_3 ceramics exhibit the highest ionic conductivity among all ZrO_2-based materials, making them promising candidates as electrolytes in intermediate-temperature solid-oxide fuel cells.

ZrO_2–Sc_2O_3 solid solutions exhibit a number of different (monoclinic, tetragonal, cubic and rhombohedral) phases that can be observed at room temperature,[1–3] but only the tetragonal and cubic ones have good ionic conductivity. For this reason, the conditions under which the tetragonal and the cubic phases can be retained were investigated by many scientists. Differently from other ZrO_2-based oxides, three different rhombohedral phases, named as β, γ and δ, have been reported in ZrO_2–Sc_2O_3 solid solutions.[1] Because of this particular feature many researchers have investigated the phase diagram of ZrO_2–Sc_2O_3 solid solutions.

In compositionally homogeneous ZrO_2-based solid solutions, the tetragonal phase takes different forms, known as t, t′ and t′′.[2–9] Besides the tetragonal t-form, which is a stable phase, t′ and t′′ are compositionally homogeneous metastable forms of the tetragonal phase that can be retained at room temperature under special conditions. The t′-form has an axial ratio, c/a, larger than unity and the t′′-form has an axial ratio, c/a, of unity, but its oxygen atoms are displaced along the c-axis from their ideal sites of the cubic phase. Yashima and coworkers have proposed a metastable-stable phase diagram for the ZrO_2–Sc_2O_3 system.[2,3] These authors studied conventional (not nanometric) samples and, at room temperature, they found a mixture of cubic and rhombohedral (β) phases within the range from 9 to 14 mol% Sc_2O_3. Different to the case of other ZrO_2-based systems, these authors did not observe the t′′-form of the tetragonal phase in compositionally homogeneous ZrO_2–Sc_2O_3 materials.

Nanostructured materials often exhibit phases and crystal structures different from those of materials with grain structures on a coarser scale. For instance, the high-temperature tetragonal phase can be retained at room temperature in nanocrystalline ZrO_2.[10–14] Recently, we have studied the metastable phases in nanocrystalline ZrO_2–Sc_2O_3 solid solutions synthesized by a new nitrate-lysine gel combustion route, for average crystallite sizes of $\langle D \rangle$ = 10 and 25 nm and compositions ranging from 1 to 13 mol% Sc_2O_3.[9] According to our synchrotron X-ray powder diffraction (SXPD) and Raman spectroscopy studies, the phases at room temperature were tetragonal t′ for compositions up to 9 mol% Sc_2O_3, tetragonal t′′ between 9 and 12 mol% Sc_2O_3 and cubic for 12 mol% Sc_2O_3 and above. The use of an intense synchrotron source for X-ray diffraction experiments was crucial to detect weak Bragg peaks related to the displacement of oxygen atoms from their positions in the cubic phase. Even though other compositionally homogeneous ZrO_2-based systems exhibit similar phases at room temperature,[4–8] our investigation showed that nanocrystalline, compositionally homogeneous ZrO_2–Sc_2O_3 materials exhibit different phases than microcrystalline ones. The main difference was that nanocrystalline samples did not exhibit the rhombohedral phases usually observed for materials with larger grains. We also determined a metastable phase diagram of ZrO_2–Sc_2O_3 solid solutions with $\langle D \rangle$ = 25 nm, finding that it strongly differs from the one proposed by Yashima and coworkers for microcrystalline compositionally homogeneous materials[2] and, also, from the equilibrium phase diagram proposed by Ruh *et al.*[1] Xu *et al*. studied ZrO_2–Sc_2O_3 nanopowders synthesized by a two step hydrothermal process.[15] In samples with very small crystallite sizes

[a] *CINSO (Centro de Investigaciones en Sólidos), CITEFA-CONICET J.B. de La Salle 4397 (B1603ALO) Villa Martelli, Pcia. de Buenos Aires, Argentina. E-mail: dlamas@citefa.gov.ar; Fax: +54-11-4709-8228; Tel: +54-11-4709-8240*
[b] *Instituto de Física, FAP, USP, Travessa R da Rua do Matão, no. 187, Cidade Universitária, (05508-900) São Paulo, Brazil. E-mail: craievich@if.usp.br*

(up to $\langle D \rangle$ = 14 nm), these authors reported the presence of the tetragonal t-phase for 4 and 6 mol% Sc_2O_3, a tetragonal t′′ phase for 8 and 10 mol% Sc_2O_3 and cubic phase for 12, 14 and 16 mol% Sc_2O_3. For samples with larger crystallite sizes these authors detected two rhombohedral phases, β and γ. Although these findings are very interesting, the authors did not provide quantitative information on phase contents and crystallographic parameters. Besides, their X-ray diffraction study was performed using a conventional (laboratory) diffractometer, making it difficult to observe weak Bragg peaks, due to relatively poor statistics to distinguish background and phase signals.

An open question that we will consider here is in which range of crystallite sizes the tetragonal and cubic phases are retained in nanocrystalline ZrO_2–Sc_2O_3. In other words, the question is how the metastable phase diagram discovered for ZrO_2–Sc_2O_3 nanocrystals[9] changes for increasing crystallite size and eventually approaches to the phase diagram reported for powders with much larger sizes.[2] In recent work,[16] we have presented preliminary results of a SXPD analysis on ZrO_2-10 mol% Sc_2O_3 materials treated at increasing calcination temperatures up to 1200 °C. This study indicated that the content of the stable rhombohedral β phase increases for increasing $\langle D \rangle$ values, finding a critical crystallite size for the retention of the metastable t′′-form of about 35 nm.

Following this idea, the aim of the present work is to identify and quantify the present phases and to characterize their crystal structures in ZrO_2–Sc_2O_3 nanopowders with Sc_2O_3 content from 10 to 14 mol%, as a function of the average crystallite size varying within a wide range up to about 100 nm. In order to determine the crystal structures, lattice parameters and phase fractions, Rietveld analyses of SXPD data were performed. The use of synchrotron radiation allowed data with high statistics. In addition, a qualitative analysis performed by Raman scattering is discussed to independently establish the presence of tetragonal, cubic and/or rhombohedral phases.

Experimental

Synthesis of nanocrystalline ZrO_2–Sc_2O_3 solid solutions

Nanocrystalline ZrO_2-10, 12 and 14 mol% Sc_2O_3 powders were synthesized by a stoichiometric gel-combustion route using lysine as an organic fuel. The synthesis process, as described in ref. 9, starts by dissolving $Zr(NO_3)_2{\cdot}6H_2O$ (Alpha Aesar, USA, 99.9%) and $Sc(NO_3)_3{\cdot}4H_2O$ (Standford Materials, USA, 99.99%) in distilled water, in the corresponding molar ratio to the desired final compositions. The amount of lysine (Merck, Germany) needed for a stoichiometric combustion reaction is then added to the solution and it is concentrated in a hot plate at 200 °C until a viscous gel is formed. Under further heating, a moderate exothermic reaction takes place.

During the whole process no precipitation was observed thus granting the homogeneity of the system. The as-reacted materials were calcined in air at 650 °C for 2 h to remove the carbonaceous residues. In order to obtain samples with different average crystallite sizes, the powders were additionally heat-treated for 1 h in air at different temperatures, namely 850, 935, 1000 and 1200 °C.

Phase identification and structural characterization

The crystalline structures of the as-synthesized and calcined nanopowders were studied by SXPD using the D10B-XPD beamline of the Brazilian Synchrotron Light Laboratory (LNLS, Campinas, Brazil).[17] SXPD measurements were performed at room temperature using an X-ray beam with a wavelength set at 1.5495 Å. A high-intensity configuration without crystal analyzer was employed in order to allow the detection of very weak Bragg reflections, particularly the 112 peak of the tetragonal structure.[7]

Rietveld refinements of SXPD patterns were performed by using the program *FullProf*.[18] This technique provided information on the structural parameters and the fraction of each component phase in multiphasic samples. Several phases were detected, namely tetragonal, cubic and rhombohedral β and/or rhombohedral γ, depending on Sc_2O_3 content and average crystallite sizes.

For Rietveld analysis, the tetragonal phase was assumed to belong to the $P4_2/nmc$ space group with the cations (Zr^{4+}, Sc^{3+}) and the O^{2-} anions in 2a and 4d positions, respectively. The lattice parameters will be given in terms of the usual pseudo-fluorite unit cell.[19] For the cubic phase, the space group was considered to be $Fm\bar{3}m$, with cations and anions in 4a and 8c positions, respectively. In the case of the rhombohedral β and γ phases, the assigned space group was $R\bar{3}$. The β phase was refined according to the crystal structure determined by Wurst *et al.*[20] with cations and anions in 18f and 6c positions. In the γ phase the cations are in 18f and the anions in 3a positions, according to Thornber *et al.*[21] The peak shape was modeled as a pseudo-Voigt function. The background of the profiles was adjusted by using a six-parameter polynomial function in $(2\theta)^n$, n = 0–5. Isotropic atomic temperature parameters were used. Equal thermal parameters for Zr and Sc and for all phases in the cases of mixtures were assumed, with the purpose of reducing the number of parameters. Under these hypotheses, Rietveld refinements were successfully performed for all SXPD patterns.

The weight fraction of the different component phases were calculated by means of the following equation:

$$W_i = \frac{S_i(ZMV)_i}{\sum_{j=1}^{n} S_j(ZMV)_j} \quad (1)$$

where W_i is the weight fraction of the "i" phase in a mixture of n phases, S the Rietveld scale factor, Z the number of basic formula per unit cell, M the mass of the formula unit and V the unit cell volume.[22]

The average crystallite sizes, $\langle D \rangle$, of each phase for all samples were determined from the width of SXPD peaks by applying the Scherrer equation,[23] considering the instrumental broadening determined from the analysis of a LaB_6 standard (NIST-SRM 660a). In multiphasic samples with strong peaks overlapping, the results of Rietveld analysis were

used to determine the width of peaks corresponding to the different phases.

The discrimination between cubic phase and the t′′-form was achieved by measuring with high step-counting times the 112 Bragg reflection of the tetragonal structure, which is forbidden in the cubic symmetry. This weak Bragg reflection is only related to the displacement of O^{2-} anions. Therefore, the use of a powerful synchrotron X-ray beam for the measurement of X-ray diffraction data becomes of critical importance to identify the t′′-form.[7]

The above SXPD analysis was complemented by Raman scattering. Raman spectra in the wave number range of 150–900 cm^{-1} were obtained in a Renishaw Imaging Microscope System 3000 spectrophotometer equipped with an Olympus BH-2 microscope and a CCD detector. The excitation source was a 632.8 nm He-Ne laser line (Spectra Physics, model 127). Spectra were acquired by averaging five scans of 20 s duration each.

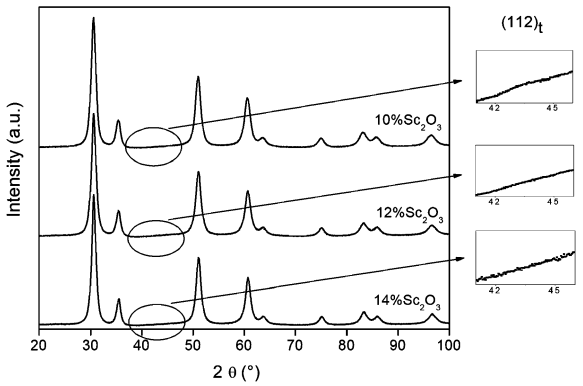

Fig. 1 SXPD patterns of ZrO_2-10, 12 and 14 mol% Sc_2O_3 nanopowders with average crystallite sizes of about 10 nm. Insets: SXPD patterns close to the 112 Bragg reflection corresponding to the t′′-form. This reflection is apparent in the 10 mol% Sc_2O_3 sample and vanishes in the 12 and 14 mol% Sc_2O_3 materials. The increasing trend of the background near the 112 peak is an effect coming from the very large width of the 220 one.

Results

SXPD analysis

The ZrO_2–Sc_2O_3 samples studied in this work, calcined at increasing temperatures up to 1200 °C, exhibited average crystallite sizes, ⟨D⟩, in the range of 8.5–110 nm, as determined by using the Scherrer equation. As we will see later, samples having smaller ⟨D⟩, up to about 25 nm, were single-phased, exhibiting the t′′-form or the cubic structure. In contrast, samples with larger ⟨D⟩ were multiphasic. The phases identified for the different Sc_2O_3 contents and calcination temperatures studied in this work, their respective weight fractions and ⟨D⟩ values are summarized in Table 1 (in some cases, as it will be explained in the following section, Raman spectroscopy data were needed to distinguish between the t′′-form and the cubic phase). It can be noticed that the values of ⟨D⟩ for different calcination temperatures are approximately independent of the Sc_2O_3 content, in the ranges of 8.5–9.5, 22–24, 29–45, 55–65 and 80–110 nm for samples calcined at 650, 850, 935, 1000 and 1200 °C, respectively. In the following discussion, we will assume typical values of ⟨D⟩ of 10, 25, 35, 60 and 100 nm, respectively, for the three Sc_2O_3 contents (10, 12 and 14 mol%) analyzed in this work.

The SXPD patterns corresponding to the samples calcined at 650 °C (*i.e.* with average crystallite size of about ⟨D⟩ ≈ 10 nm) are displayed in Fig. 1. By examining these patterns it can easily be seen that all samples are single-phased and that all strong X-ray Bragg reflections (111, 200, *etc.*) can be indexed by assuming a faced centered cubic (fcc) unit cell. As it can be observed in the inset at the top of Fig. 1, the 112 reflection was present for the 10 mol% Sc_2O_3 sample. The presence of this weak reflection reveals that the structure of this sample corresponds to the tetragonal t′′-form, with a cubic unit cell but with the oxygen anions slightly displaced from their positions expected for a fluorite-type cubic structure. The fractional *z*-coordinate of the O^{2-} anion in the asymmetric unit of the tetragonal unit cell, *z*(O), determined from the ratio

Table 1 Phases identified by SXPD and Raman spectroscopy, phase contents determined by quantitative Rietveld analysis and average crystallite sizes determined by Scherrer equation for all ZrO_2–Sc_2O_3 powders analyzed in this work. Numbers in parentheses indicate the error in the last significant digit

			Average crystallite size/nm			Phase contents (wt.%)		
Sc_2O_3 content (mol%)	Calcination *T*/°C	Identified phases	t′′/c	β	γ	t′′/c	β	γ
10	650	*t′′*	8.5(6)	—	—	100	—	—
	850	*t′′*	24(2)	—	—	100	—	—
	935	*t′′* + β	29(2)	38(3)	—	50(1)	50(1)	—
	1000	*t′′* + β	60(5)	65(5)	—	22.0(4)	78.0(7)	—
	1200	c (or *t′′*) + β[a]	1.0(1)*10^2	1.0(1)*10^2	—	15.2(4)	84.8(9)	—
12	650	c	9.0(7)	—	—	100	—	—
	850	c	24(2)	—	—	100	—	—
	935	β + γ + c	45(4)	42(4)	33(3)	39(1)	40(1)	21(1)
	1000	β + γ + c	55(5)	65(6)	55(5)	23(1)	55(1)	22(1)
	1200	β + γ	—	80(7)	90(9)	—	83.7(9)	16.3(5)
14	650	c	9.5(7)	—	—	100	—	—
	850	c	22(2)	—	—	100	—	—
	935	c + γ	36(4)	—	42(4)	40(1)	—	60(1)
	1000	γ + β	—	60(5)	65(6)	—	13.5(5)	86.5(9)
	1200	γ + β	—	80(8)	1.1(1)*10^2	—	11.8(3)	88.2(8)

[a] In this sample, Raman spectroscopy data are not clear enough to discriminate between the cubic phase and the t′′-form of the tetragonal phase.

of the integrated intensities of the 112 and 111 peaks, resulted in 0.237(2). On the other hand, the other insets of Fig. 1 indicate that the 12 and 14 mol% Sc_2O_3 samples do not show any trace of the 112 peak, thus, these powders exhibited the cubic phase.

Similar to the SXPD patterns corresponding to the nanopowders with $\langle D \rangle \approx 10$ nm, the analysis of SXPD data for those with $\langle D \rangle \approx 25$ nm (calcined at 850 °C) confirmed that they also exhibited the t′′-form for 10 mol% Sc_2O_3 and the cubic phase for 12 and 14 mol% Sc_2O_3. The value of z(O) for the 10 mol% Sc_2O_3 sample calcined at 850 °C resulted in 0.237(2), the same value determined for the sample calcined at 650 °C.

The analysis of SXPD data corresponding to nanopowders with $\langle D \rangle$ above 25 nm (*i.e.* calcined at 935 °C or higher temperatures) demonstrated that these samples exhibited a mixture of two or three different phases. This can be clearly observed in Fig. 2, which shows the 2θ region close to the 220 peak of the t′′-form or the cubic phase for nanopowders with different Sc_2O_3 contents and calcination temperatures. Bragg reflections in these SXPD patterns were assigned to either cubic or rhombohedral, β or γ phases, depending on Sc_2O_3 content and $\langle D \rangle$. For these samples with large $\langle D \rangle$, it was not possible to discriminate between the t′′-form and the cubic phase by means of SXPD, because the very weak Bragg peaks, characteristics of the t′′-form, are strongly overlapped with peaks corresponding to the rhombohedral phases. Therefore, in the following analysis of samples with large $\langle D \rangle$, we assumed the cubic phase. However, in some cases, the Raman spectroscopy data made possible to distinguish both phases.

For samples with 10 mol% Sc_2O_3, the 220 Bragg peak of the t′′-form in Fig. 2 splits into two peaks that can be assigned to a rhombohedral β phase. For the 12 mol% Sc_2O_3 ones, the 220 peak of the cubic phase changes to four well-resolved peaks, two of them belonging to the rhombohedral β phase and the other two to the rhombohedral γ one. The SXPD patterns of ZrO_2-14 mol% Sc_2O_3 materials exhibit similar features to those of ZrO_2-12 mol% Sc_2O_3 samples, but the Bragg peaks of the γ phase are stronger. In all cases, the integrals of the Bragg peaks of the t′′-form and cubic phase decrease for increasing calcination temperature, *i.e.* for increasing $\langle D \rangle$.

The crystallographic parameters determined from Rietveld analysis for the different phases of all samples are listed in Table 2. The atomic positions determined by Wurst *et al.*[20] for the β phase and by Thornber *et al.*[21] for the γ one were fixed in all cases and led to good fittings of both, strong and weak, Bragg reflections. For example, Fig. 3 shows a typical and excellent agreement obtained between experimental data and fit for the ZrO_2-12 mol% Sc_2O_3 sample calcined at 935 °C. The calculated lattice parameters determined here are in accordance with those published in the literature.[2,3,20,21]

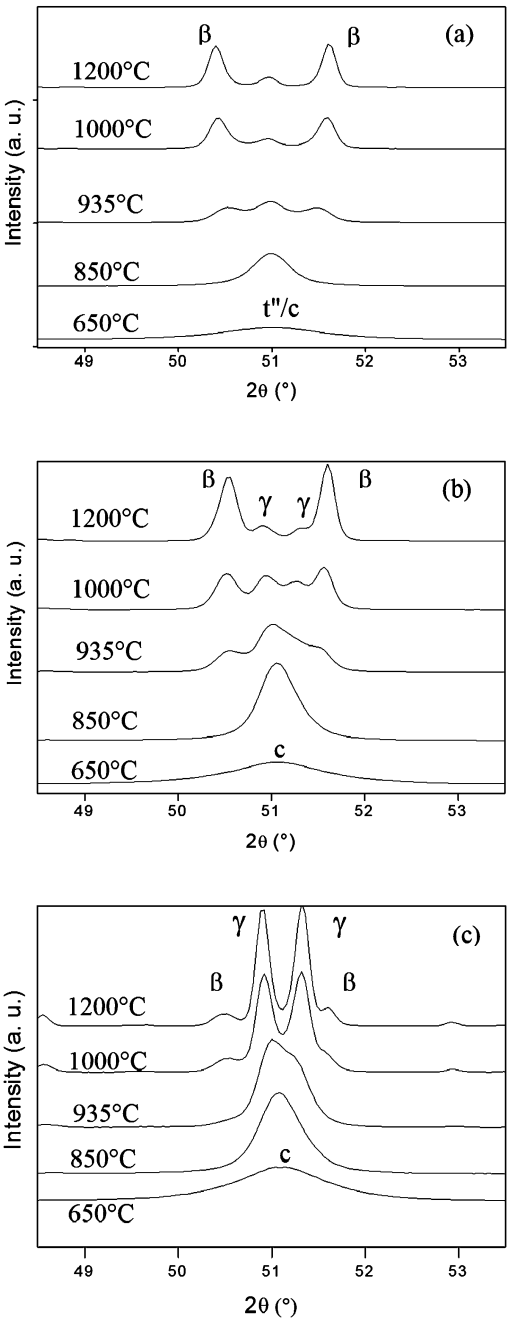

Fig. 2 SXPD patterns close to the 220 Bragg peak of the t′′-form or the cubic phase for nanopowders with different Sc_2O_3 contents and calcination temperatures (or average crystallite sizes). (a) ZrO_2-10 mol% Sc_2O_3 samples; (b) ZrO_2-12 mol% Sc_2O_3 samples; (c) ZrO_2-14 mol% Sc_2O_3 samples.

Raman spectroscopy

Our Raman scattering measurements, displayed in Fig. 4, confirmed the existence of different phases previously identified by SXPD and provided complementary information about their detailed features. Raman scattering results were particularly helpful to distinguish between the t′′-form (tetragonal phase with a cubic unit cell) and the cubic phase in multiphasic samples, for which SXPD data were not conclusive since the weak 112 Bragg peak is masked by other Bragg reflections associated to β and/or γ phases.

The band at about 470 cm^{-1} (marked with a star) is considered as a signature of the tetragonal structure.

Table 2 Results obtained from Rietveld refinements of SXPD data for ZrO_2-10, 12 and 14 mol% Sc_2O_3 powders analyzed in this work. Numbers in parentheses indicate the error in the last significant digit. The isotropic Debye–Waller factors for Zr and Sc atoms were assumed to be equal. For multiphasic samples, these Debye–Waller factors were considered equal for all phases

Sc_2O_3 content (mol%)	Calcination T/°C	Phase	Space group	a/Å	c/Å	B(Zr,Sc)/Å^2	B(O)/Å^2	R_p	R_{wp}	R_{exp}
10	650	t″	$P4_2/nmc$	5.0878(4)	5.089(1)	1.05(4)	2.4(1)	5.89	7.9	2.46
	850	t″	$P4_2/nmc$	5.0887(3)	5.0891(7)	0.99(2)	2.72(7)	6.07	8.01	2.41
	935	c[a]	$Fm\bar{3}m$	5.08864(5)		0.60(3)	1.70(8)	7.33	9.44	2.31
		β	$R\bar{3}$	19.8531(3)	17.9404(2)					
	1000	c[a]	$Fm\bar{3}m$	5.09284(3)		0.38(3)	1.10(9)	8.48	11.0	2.26
		β	$R\bar{3}$	19.8244(1)	18.00867(9)					
	1200	c	$Fm\bar{3}m$	5.09189(2)		0.39(9)	0.23(3)	9.1	11.5	2.24
		β	$R3$	19.8153(1)	18.02770(7)					
12	650	c	$Fm\bar{3}m$	5.0850(1)		1.21(3)	2.94(8)	6.32	5.54	2.04
	850	c	$Fm\bar{3}m$	5.08396(5)		1.21(3)	3.03(9)	11.1	12.8	2.42
	935	c	$Fm\bar{3}m$	5.08321(5)		0.67(3)	1.35(8)	7.88	9.54	2.38
		β	$R\bar{3}$	19.8476(3)	17.9311(2)					
		γ	$R\bar{3}$	9.5368(1)	17.4798(2)					
	1000	c	$Fm\bar{3}m$	5.08351(4)		0.50(3)	0.20(9)	9.43	11.5	2.32
		β	$R\bar{3}$	19.8305(2)	17.9550(1)					
		γ	$R\bar{3}$	9.5381(1)	17.4781(2)					
	1200	β	$R\bar{3}$	19.8266(1)	17.963(1)	0.26(4)	0.1(1)	11.5	14.4	2.3
		γ	$R\bar{3}$	9.5409(9)	17.4792(2)	0.26(4)	0.1(1)			
14	650	c	$Fm\bar{3}m$	5.07838(1)		1.34(4)	3.22(9)	7.01	9.09	2.7
	850	c	$Fm\bar{3}m$	5.08254(6)		1.38(3)	3.41(8)	9.3	11.0	2.58
	935	c	$Fm\bar{3}m$	5.08550(4)		0.80(3)	1.55(8)	8.44	10.1	2.46
		γ	$R\bar{3}$	9.5399(1)	17.4869(2)					
	1000	β	$R\bar{3}$	19.8538(2)	17.9736(2)	0.13(9)	0.41(3)	9.63	12.0	2.32
		γ	$R\bar{3}$	9.54114(6)	17.48248(9)					
	1200	β	$R\bar{3}$	19.8297(1)	17.9900(1)	0.29(3)	0.03(9)	9.48	11.8	2.38
		γ	$R\bar{3}$	9.54110(4)	17.46648(6)					

[a] For these samples, in spite of the results of Raman spectroscopy, we used a fluorite-like cubic phase instead of the t''-form of the tetragonal phase (this means that we ignored the small effect of oxygen displacements) in order to simplify the structural model.

Its presence for ZrO_2-10 mol% Sc_2O_3 nanopowders with $\langle D \rangle \approx 10$ and 25 nm implied that these samples exhibit the tetragonal phase (see Fig. 4(a)), thus confirming SXPD analysis. The band at 470 cm^{-1} is also apparent in Raman spectra of samples with $\langle D \rangle \approx 35$ and 60 nm (calcined at 935 and 1000 °C, respectively), while its presence is not clear in the spectrum corresponding to $\langle D \rangle \approx 100$ nm, so in this last sample we could not discriminate between the t″-form and the cubic phase. Raman bands at 310, 350, 485, 522, 585 and 606 cm^{-1} observed in the spectra of samples with $\langle D \rangle \approx 35$, 60 and 100 nm (marked with ●) were assigned to the β-phase.[3]

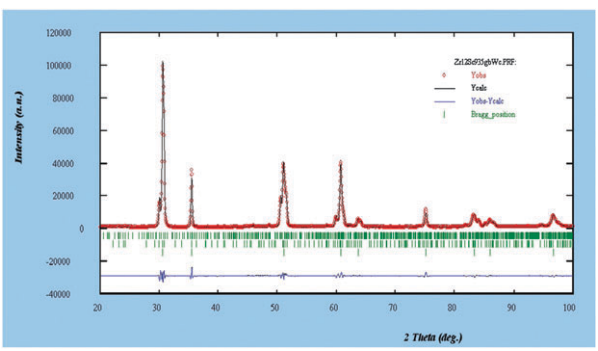

Fig. 3 Agreement between experimental SXPD data and fit obtained after Rietveld refinements for the ZrO_2-12 mol% Sc_2O_3 sample calcined at 935 °C. Data, fit and difference are indicated in red, black and blue, respectively.

In the case of the ZrO_2-12 mol% Sc_2O_3 samples (Fig. 4(b)), the tetragonal phase cannot be clearly detected because the 470 cm^{-1} band is weak and much larger than those observed for the spectra corresponding to samples with ZrO_2-10 mol% Sc_2O_3. Hence the ZrO_2-12 mol% Sc_2O_3 with $\langle D \rangle \approx 10$ and 25 nm were characterized as cubic instead of tetragonal. The spectra of samples with $\langle D \rangle \approx 35$, 60 and 100 nm (calcined at 935, 1000 and 1200 °C, respectively) exhibit additional peaks at 295, 408, 432, 520 and 560 cm^{-1} (marked with □) that were assigned to the γ phase.[15]

The absence of the 470 cm^{-1} Raman band for the ZrO_2-14 mol% Sc_2O_3 sample with $\langle D \rangle \approx 10$ nm (Fig. 4(c)) indicates that this sample also exhibits the cubic phase, while the presence of Raman bands corresponding to γ phase have been identified in the spectra associated to samples with average sizes $\langle D \rangle \approx 35$ nm and larger.

Discussion

Our experimental results allowed us not only to identify the phases retained in the ZrO_2–Sc_2O_3 system for different compositions and average crystallite sizes, but also to provide detailed quantitative information regarding the retention of metastable phases in these materials. This important new quantitative information is summarized in Fig. 5, a 3D-diagram that indicates the weight fractions of c/t″, β and γ phases as functions of Sc_2O_3 content and $\langle D \rangle$. This diagram shows that single-, two- or three-phase materials can be obtained. In particular, it shows that the metastable t″-form

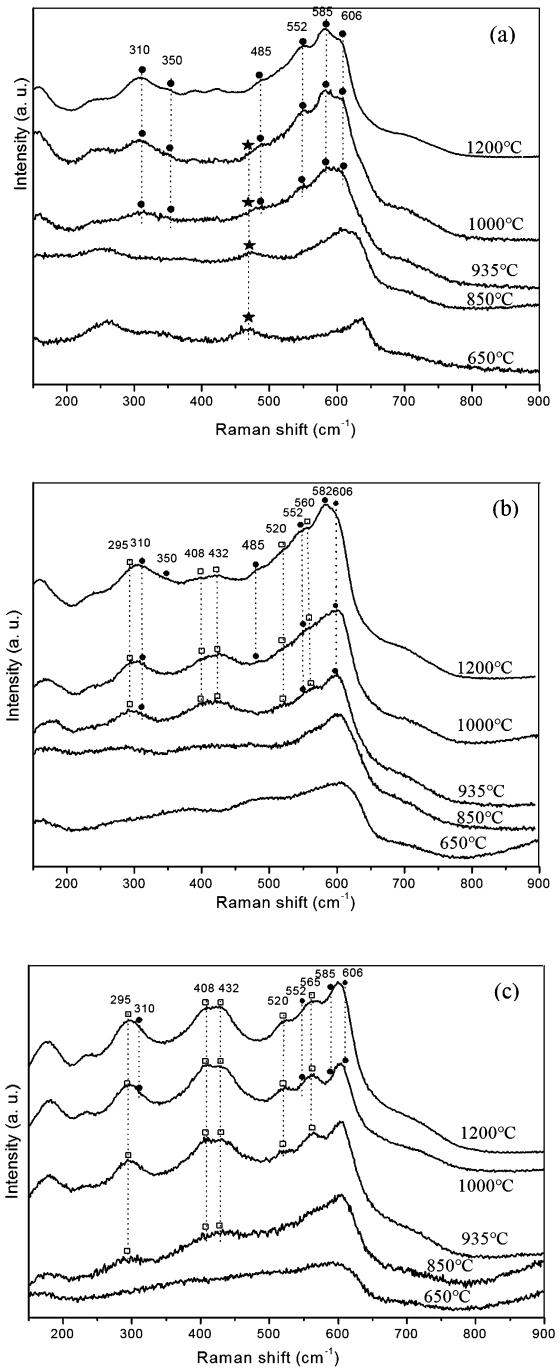

Fig. 4 Raman spectra of ZrO_2–Sc_2O_3 samples for the different average crystallite sizes and compositions analyzed in this work. (a) ZrO_2-10 mol% Sc_2O_3 samples; (b) ZrO_2-12 mol% Sc_2O_3 samples; (c) ZrO_2-14 mol% Sc_2O_3 samples. The stars indicate the Raman band at 470 cm^{-1} associated to a tetragonal structure. The filled circles (●) indicate the Raman bands associated to rhombohedral β phase and the open squares (□) indicate those corresponding to the rhombohedral γ phase.

and the cubic phase can only be retained for materials with small ⟨D⟩, resulting in a critical size of about 30–40 nm for the compositional range considered in this investigation. Therefore, we can conclude that the materials gradually approach to the behavior predicted by the equilibrium phase diagram as ⟨D⟩ grows, while the phase fractions depend on ⟨D⟩ and composition.

2D-plots that report the results of our quantitative analyses as functions of ⟨D⟩ for the three Sc_2O_3 contents studied in this work are also shown in Fig. 5. Their main features are the following:

(i) ZrO_2-10 mol% Sc_2O_3: the t′′-form of the tetragonal phase is fully retained for ⟨D⟩ up to 25 nm (calcined up to 850 °C), whereas the content of this phase decreases from 50 to 15 wt.% for increasing ⟨D⟩ from about 35 nm up to 100 nm. Correspondingly, the content of rhombohedral β phase gradually increases from 50 to 85 wt.%.

(ii) ZrO_2-12 mol% Sc_2O_3: the cubic phase is fully retained in samples with ⟨D⟩ up to 25 nm. For larger ⟨D⟩, the cubic phase coexists with the rhombohedral phases and its content decreases from 39 down to 0 wt.%, for materials with ⟨D⟩ increasing from ≈ 35 nm up to ≈ 100 nm. The β phase appears for ⟨D⟩ ≈ 35 nm and its content gradually grows for increasing ⟨D⟩ up to 84 wt.% for ⟨D⟩ ≈ 100 nm. The γ phase also appears in samples with ⟨D⟩ ≥ 35 nm and its content varies between 16–22 wt.%.

(iii) ZrO_2-14 mol% Sc_2O_3: all the features of this composition are similar to those of the ZrO_2-12 mol% Sc_2O_3 materials, but the γ phase dominates in materials with large ⟨D⟩ instead of the β phase.

Conclusions

The combined application of SXPD and Raman scattering allowed us to identify and quantify the phases present in nanocrystalline ZrO_2–Sc_2O_3 materials with Sc_2O_3 contents from 10 up to 14 mol% and average crystallite sizes ranging from about 10 up to 100 nm.

This investigation established that the t′′-form or the cubic phase are fully retained in nanopowders composed of very small crystallites of ZrO_2–Sc_2O_3 with ⟨D⟩ up to 25 nm. The t′′-form was identified in samples with 10 mol% Sc_2O_3 and the cubic phase in samples with 12 and 14 mol% Sc_2O_3. These nanopowders with the smallest crystallite sizes (⟨D⟩ ≈ 10 nm and 25 nm) are single phased, essentially free from any significant contribution from the stable rhombohedral phases.

ZrO_2-10, 12 and 14 mol% Sc_2O_3 materials with ⟨D⟩ ≥ 35 nm are multiphasic. In samples with increasing average crystallite size, the content of t′′-form or cubic phase decreases while the weight fraction of β and γ rhombohedral phases increases. Thus, the system progressively approaches to the known phase diagram of materials with large (micrometric) crystallites.

Finally, we remind that the tetragonal and cubic phases that have being retained at room temperature in the studied nanostructured ZrO_2–Sc_2O_3 powders exhibit better electrical properties than the stable rhombohedral phases. However, practical use of the studied powders as precursors of dense ceramic materials for industrial applications requires additional studies to verify the stability of the retained tetragonal or cubic phases under real processing conditions. The investigation of the crystallographic structure of sintered ceramics and the analysis of the local structure of this system, determined from X-ray

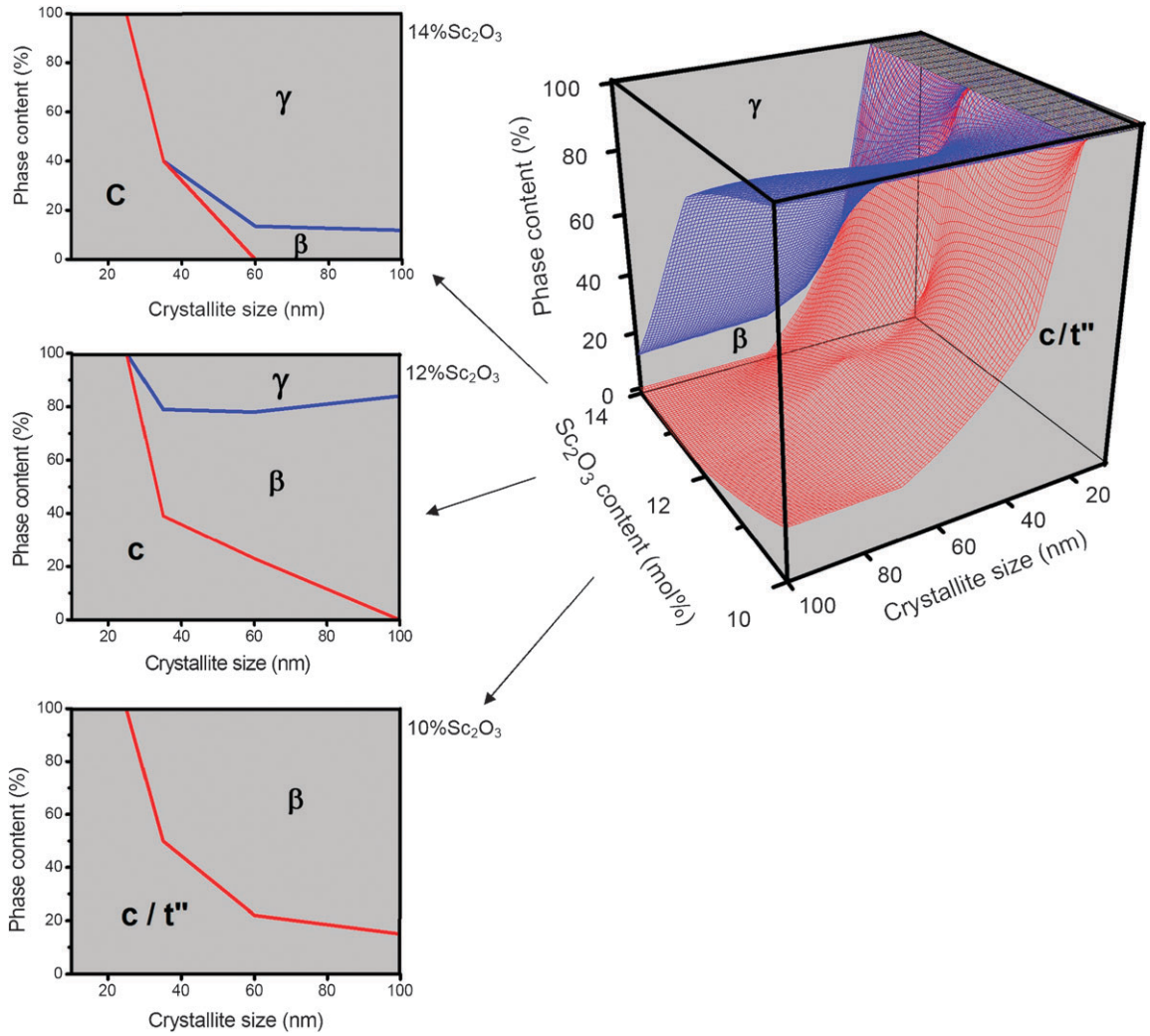

Fig. 5 Content (weigh fraction) of c/t′′, β and γ phases for nanocrystalline ZrO_2–Sc_2O_3 materials with Sc_2O_3 contents between 10 and 14 mol% and average crystallite sizes ranging from 10 to 100 nm. The 2D-plots correspond to the three compositions analyzed in this work: ZrO_2-10, 12 and 14 mol% Sc_2O_3.

absorption spectroscopy, are under way. These investigations are expected to shine a light on structural changes as a function of composition and crystallite size and also on the correlation between the short and long range atomic order in the studied materials.

Acknowledgements

The authors thank Dr M. L. A. Temperini for helping with Raman spectroscopy measurements. This work was supported by the Brazilian Synchrotron Light Laboratory (LNLS, Brazil, proposals D10B-XPD-5364, 6723 and 7296), the scientific collaboration projects CNPq-CONICET and CAPES-MinCyT (Brazil-Argentina), CNPq (Brazil, PROSUL programs 490289/2005-3 and 490580/2008-4), Agencia Nacional de Promoción Científica y Tecnológica (Argentina, PICT 2005 No. 38309 and PICT 2007 No. 01152), CONICET (Argentina, PIP No. 6559) and Latin-American Centre for Physics (CLAF). P. M. Abdala thanks CONICET and YPF foundation for her doctoral fellowship.

Notes and references

1 R. Ruh, H. J. Garrett, R. F. Domagala and V. A. Patel, *J. Am. Ceram. Soc.*, 1977, **60**, 399.
2 M. Yashima, M. Kakihana and M. Yoshimura, *Solid State Ionics*, 1996, **86–88**, 1131.
3 H. Fujimori, M. Yashima, M. Kakihana and M. Yoshimura, *J. Am. Ceram. Soc.*, 1998, **81**, 2885.
4 M. Yashima, S. Sasaki, M. Kakihana, Y. Yamaguchi, H. Arashi and M. Yoshimura, *Acta Crystallogr., Sect. B: Struct. Sci.*, 1994, **50**, 663.
5 M. Yashima, K. Ohtake, M. Kakihana, H. Arashi and M. Yoshimura, *J. Phys. Chem. Solids*, 1996, **57**, 17.
6 M. Yashima, S. Sasaki, Y. Yamaguchi, M. Kakihana, M. Yoshimura and T. Mori, *Appl. Phys. Lett.*, 1998, **72**, 182.
7 D. G. Lamas, R. O. Fuentes, I. O. Fábregas, M. E. Fernández de Rapp, G. E. Lascalea, J. R. Casanova, N. E. Walsöe de Reca and A. F. Craievich, *J. Appl. Crystallogr.*, 2005, **38**, 867.
8 I. O. Fábregas, D. G. Lamas, N. E. Walsöe de Reca, M. C. A. Fantini, A. F. Craievich and R. J. Prado, *J. Appl. Crystallogr.*, 2008, **41**, 680.
9 P. M. Abdala, A. F. Craievich, M. C. A. Fantini, M. L. A. Temperini and D. G. Lamas, *J. Phys. Chem. C*, 2009, **113**, 18661.
10 R. C. Garvie, *J. Phys. Chem.*, 1965, **69**, 1238.
11 R. C. Garvie, *J. Phys. Chem.*, 1978, **82**, 218.

12 R. Nitschea, M. Rodewalda, G. Skandanb, H. Fuessa and H. Hahna, *Nanostruct. Mater.*, 1996, **7**, 535.
13 S. Shukla, S. Seal, R. Vij, S. Bandyopadhyay and Z. Rahman, *Nano Lett.*, 2002, **2**, 989.
14 D. G. Lamas, A. M. Rosso, M. Suarez Anzorena, A. Fernández, M. G. Bellino, M. D. Cabezas, N. E. Walsöe de Reca and A. F. Craievich, *Scr. Mater.*, 2006, **55**, 553.
15 G. Xu, Y. W. Zhang, C. S. Liao and C. H. Yan, *Phys. Chem. Chem. Phys.*, 2004, **6**, 5410.
16 P. M. Abdala, D. G. Lamas, M. C. A. Fantini and A. F. Craievich, *J. Alloys Compd.*, 2009, DOI: 10.1016/j.jallcom.2009.08.083, in press.
17 F. F. Ferreira, E. Granado, W. Carvalho, Jr., S. W. Kycia, D. Bruno and R. Droppa, Jr., *J. Synchrotron Rad.*, 2006, **13**, 46.
18 J. Rodríguez-Carvajal, *FullProf 98, version 0.2*, Laboratoire Léon Brillouin (CEA-CNRS), Saclay, France, 1998.
19 W. E. Lee and W. M. Rainforth, *Ceramic Microstructures: Property Control by Processing*, Chapman & Hall, London, 1994;, p. 317.
20 K. Wurst, E. Schweda, D. J. M. Bevan, J. Mohyla, K. S. Wallwork and M. Hofmann, *Solid State Sci.*, 2003, **5**, 1491.
21 M. R. Thornber, D. J. M. Bevan and J. Graham, *Acta Crystallogr., Sect. B: Struct. Crystallogr. Cryst. Chem.*, 1968, **24**, 1183.
22 R. A. Young, *The Rietveld Method*, Oxford University Press, Oxford, 1993.
23 H. Klug and L. Alexander, *X-ray Diffraction Procedures for Polycrystalline and Amorphous Materials*, second ed., John Wiley and Sons, New York, 1974.